Valley-Polarized Metals and Quantum Anomalous Hall Effect in Silicene

Motohiko Ezawa

Department of Applied Physics, University of Tokyo, Hongo 7-3-1, 113-8656, Japan

(Received 3 March 2012; published 1 August 2012)

Silicene is a monolayer of silicon atoms forming a two-dimensional honeycomb lattice, which shares almost every remarkable property with graphene. The low-energy structure of silicene is described by Dirac electrons with relatively large spin-orbit interactions due to its buckled structure. The key observation is that the band structure is controllable by applying electric field to silicene. We explore the phase diagram of silicene together with exchange field M and by applying electric field E_z. A quantum anomalous Hall (QAH) insulator, valley polarized metal (VPM), marginal valley polarized metal (M-VPM), quantum spin Hall insulator, and band insulator appear. They are characterized by the Chern numbers and/or by the edge modes of a nanoribbon. It is intriguing that electrons have been moved from a conduction band at the K point to a valence band at the K' point for $E_z > 0$ in the VPM. We find in the QAH phase that almost flat gapless edge modes emerge and that spins form a momentum-space Skyrmion to yield the Chern number. It is remarkable that a topological quantum phase transition can be induced simply by changing electric field in a single silicene sheet.

DOI: 10.1103/PhysRevLett.109.055502 PACS numbers: 81.05.ue, 72.25.Dc, 72.80.Vp, 73.20.At

Silicene, a monolayer of silicon atoms forming a two-dimensional honeycomb lattice, has been synthesized [1–3] and attracts much attention [4–8] recently. Almost every striking property of graphene could be transferred to this innovative material. It has, additionally, a salient feature, that is a buckled structure [4,5], owing to a large ionic radius of silicon. Silicene has a relatively large spin-orbit (SO) gap of 1.55 meV, which provides a mass to Dirac electrons. Furthermore, we may control experimentally the mass [7] by applying the electric field E_z. Silicene undergoes a topological phase transition from a quantum spin Hall (QSH) state to a band insulator (BI) as $|E_z|$ increases [7]. A QSH state is characterized by a full insulating gap in the bulk and helical gapless edges [9–12].

There exits another state of matter in graphene [13–15], that is a quantum anomalous Hall (QAH) state [16–19], characterized by a full insulating gap in the bulk and chiral gapless edges. Unlike the quantum Hall effect, which arises from Landau-level quantization in a strong magnetic field, the QAH effect is induced by internal magnetization and SO coupling.

In this paper we analyze the band structure of silicene together with exchange field M and by applying electric field E_z to silicene. We explore the phase diagram in the E_z-M plane. Silicene has a rich varieties of phases because the electric field E_z and the exchange field M have different effects on the conduction and valence bands characterized by the spin and valley indices. There are insulator phases, which are the QSH, QAH, and BI phases. There emerges a new type of metal phase, the valley-polarized metal (VPM) phase, where electrons have been moved from a conduction band at the K point to a valence band at the K' point for $E_z > 0$. Such a phase is utterly unknown in literature as far as we are aware of. There are also metallic states on phase boundaries, which are metal (M), marginal-VPM (M-VPM) and spin VPM (SVPM) states. All these phases and states are characterized by the Chern numbers and/or by the edge modes of a nanoribbon. It is possible to materialize any one of them by controlling E_z at an appropriate value of M. Furthermore, as we have pointed out elsewhere [7], by applying an inhomogeneous field E_z, it is possible to materialize some of these topological phases together with states on the phase boundaries simultaneously in a single silicene sheet.

Silicene consists of a honeycomb lattice of silicon atoms with two sublattices made of A sites and B sites. The states near the Fermi energy are π orbitals residing near the K and K' points at opposite corners of the hexagonal Brillouin zone. We refer to the K or K' point also as the K_η point with the valley index $\eta = \pm 1$. We take a silicene sheet on the xy plane, and apply the electric field E_z perpendicular to the plane. Due to the buckled structure the two sublattice planes are separated by a distance, which we denote by 2ℓ with $\ell = 0.23$ Å. It generates a staggered sublattice potential $\propto 2\ell E_z$ between silicon atoms at A sites and B sites.

The silicene system is described by the four-band second-nearest-neighbor tight binding model,

$$\begin{aligned} H = & -t\sum_{\langle i,j\rangle\alpha} c_{i\alpha}^\dagger c_{j\alpha} + i\frac{\lambda_{\rm SO}}{3\sqrt{3}}\sum_{\langle\langle i,j\rangle\rangle\alpha\beta}\nu_{ij}c_{i\alpha}^\dagger\sigma_{\alpha\beta}^z c_{j\beta} \\ & + i\lambda_{\rm R1}(E_z)\sum_{\langle i,j\rangle\alpha\beta} c_{i\alpha}^\dagger(\boldsymbol{\sigma}\times\hat{\boldsymbol{d}}_{ij})_{\alpha\beta}^z c_{j\beta} \\ & - i\frac{2}{3}\lambda_{\rm R2}\sum_{\langle\langle i,j\rangle\rangle\alpha\beta}\mu_i c_{i\alpha}^\dagger(\boldsymbol{\sigma}\times\hat{\boldsymbol{d}}_{ij})_{\alpha\beta}^z c_{j\beta} \\ & - \ell\sum_{i\alpha}\mu_i E_z c_{i\alpha}^\dagger c_{i\alpha} + M\sum_{i\alpha} c_{i\alpha}^\dagger\sigma_z c_{i\alpha}, \end{aligned} \tag{1}$$

where $c^{\dagger}_{i\alpha}$ creates an electron with spin polarization α at site i, and $\langle i,j\rangle/\langle\langle i,j\rangle\rangle$ run over all the nearest or next-nearest neighbor hopping sites. We explain each term. (i) The first term represents the usual nearest-neighbor hopping with the transfer energy $t = 1.6$ eV. (ii) The second term represents the effective SO coupling with $\lambda_{\rm SO} = 3.9$ meV, where $\boldsymbol{\sigma} = (\sigma_x, \sigma_y, \sigma_z)$ is the Pauli matrix of spin, with $\nu_{ij} = +1$ if the next-nearest-neighboring hopping is anticlockwise and $\nu_{ij} = -1$ if it is clockwise with respect to the positive z axis. (iii) The third term represents the first Rashba SO coupling associated with the nearest neighbor hopping, which is induced by external electric field [14,20,21]. It satisfies $\lambda_{\rm R1}(0) = 0$ and becomes of the order of 10 μeV at the critical electric field $E_c = \lambda_{\rm SO}/\ell = 17$ meV Å^{-1}. (iv) The forth term represents the second Rashba SO coupling with $\lambda_{\rm R2} = 0.7$ meV associated with the next-nearest neighbor hopping term, where $\mu_i = \pm 1$ for the A (B) site, and $\hat{\boldsymbol{d}}_{ij} = \boldsymbol{d}_{ij}/|\boldsymbol{d}_{ij}|$ with the vector $\boldsymbol{d}_{ij}$ connecting two sites i and j in the same sublattice. (v) The fifth term is the staggered sublattice potential term. (vi) The sixth term represents the exchange magnetization: Exchange field M may arise due to proximity coupling to a ferromagnet such as depositing Fe atoms to the silicene surface or depositing silicene to a ferromagnetic insulating substrate, as has been argued for graphene [13–15]. The Hamiltonian (1) can also be used to describe germanene, which is a honeycomb structure of germanium [5,6], where various parameters are $t = 1.3$ eV, $\lambda_{\rm SO} = 43$ meV, $\lambda_{\rm R2} = 10.7$ meV and $\ell = 0.33$ Å.

In this Letter, we derive the topological phase diagram in the E_z-M plane and make its physical interpretation. The topological quantum numbers are the Chern number C and the $\mathbb{Z}_2$ index. If the spin s_z is a good quantum number, the $\mathbb{Z}_2$ index is identical to the spin-Chern number C_s. They are defined when the state is gapped and when the Fermi level is taken within the gap, and given by $C = C_+ + C_-$ and $C_s = \frac{1}{2}(C_+ - C_-)$, where $C_\pm$ is the summation of the Berry curvature in momentum space over all occupied states of electrons with $s_z = \pm 1$. They are well defined even if the spin is not a good quantum number [15,21,22]. In the present model, the spin is not a good quantum number because of spin mixing due to the Rashba couplings $\lambda_{\rm R1}$ and $\lambda_{\rm R2}$, and the resulting angular momentum eigenstates are indexed by the spin chirality $s = \pm 1$. We can calculate these numbers at each point in the E_z-M plane by using the standard formulas [13–15].

We present our result on the phase diagram in Fig. 1. We show later how to derive the phase boundaries based on the low-energy Dirac theory. We have also calculated the band structure of a silicene nanoribbon with zigzag edges, which we give in Fig. 2 for typical points in the phase diagram. The topological numbers are $(C, C_s) = (0, 0)$ in the BI phase, (0, 1) in the QSH phase, (2, 0) in the QAH phase with $M > 0$ and $(-2, 0)$ in the QAH phase with $M < 0$.

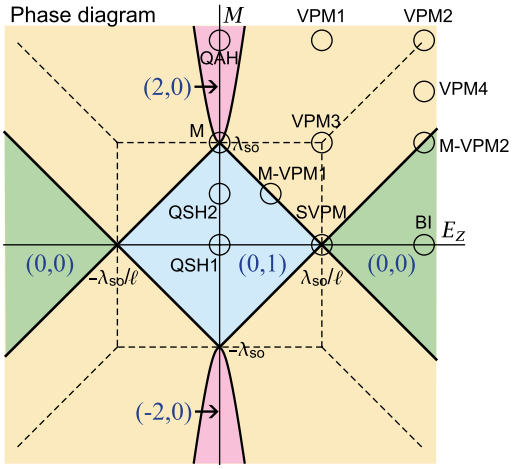

FIG. 1 (color online). Phase diagram in the E_z-M plane. Heavy lines represent phase boundaries, where the system becomes metallic. Chern and spin-Chern numbers (C, C_s) are well defined and given in insulator phases. Dotted lines represent the points where the band gap closes, which are within the VPM phase. A circle shows a point where the energy spectrum is calculated and shown in Fig. 2.

In all these states, the band gap is open, where the Fermi level is present, and they are insulators.

We first discuss the system at $E_z = 0$ and compare our results with those previously obtained in graphene [13–15]. The main difference is the appearance of almost flat edge modes in our system (Fig. 3). This occurs because the Rashba interactions are different between these two systems. We have $\lambda_{\rm R1} = 0$ for $E_z = 0$ and $\lambda_{\rm R2} = 0$ at the K and K' points in silicene, but $\lambda_{\rm R1} \neq 0$ and $\lambda_{\rm R2} = 0$ in graphene. Nevertheless, the difference is only quantitative. As far as the topological properties are concerned, there exists no difference. Indeed, in these two systems, the Chern number is identical in each corresponding phase together with quantized Hall conductivity, and the edge states support the edge current. However, the group velocity of the edge modes is extremely small due to the almost flat gapless modes in silicene.

Our most important result is the VPM phase, which appears in such regions that $E_z M \neq 0$ and occupies a major part of the phase diagram. A part of the conduction (valence) band is above (below) the Fermi level at the K (K') point for $E_z > 0$, as is observed in Fig. 2 (VPM). Hence, electrons are moved from the K valley to the K' valley, as implies the valley polarization. The phase is characterized by the property that it is a metallic state though gaps are open both at the K and K' points. We note that the Chern and spin-Chern numbers are ill-defined in the VPM phase, since the Fermi level does not lie inside the band gaps at the K and K' points simultaneously.

There exist M-VPM states on phase boundaries indicated by heavy lines in the phase diagram, where the conduction and valence bands touch the Fermi surface at the K and K' points, respectively, for $E_z > 0$. On the other hand, in

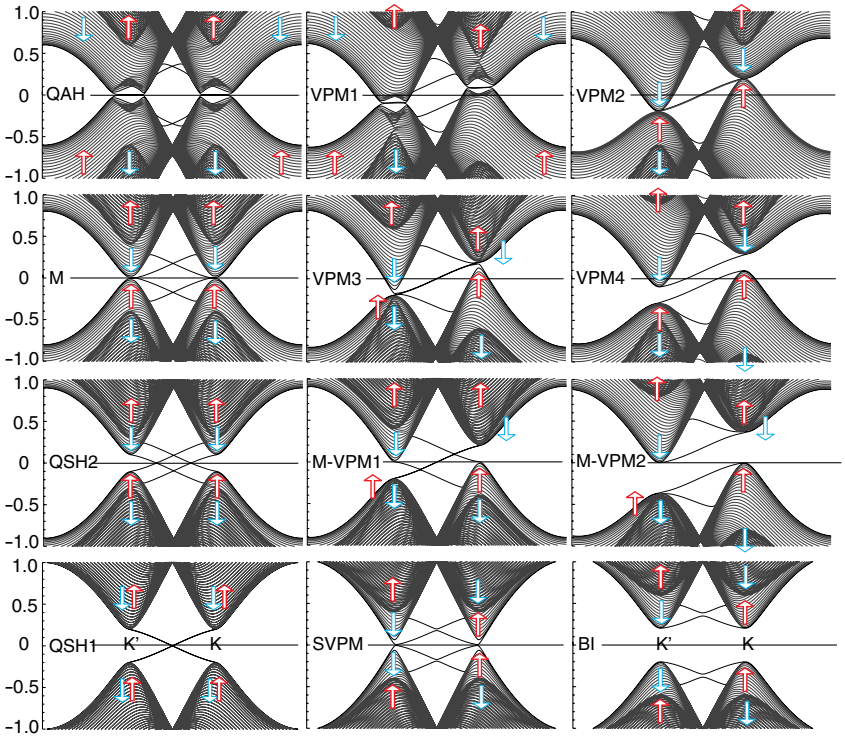

FIG. 2 (color online). The band structure of a silicene nanoribbon at marked points in the phase diagram (Fig. 1). The vertical axis is the energy in unit of t, and the horizontal axis is the momentum. We can clearly see the Dirac cones representing the energy spectrum of the bulk, as explained in Fig. 3. Lines connecting the two Dirac cones are edge modes. The spin s_z is practically a good quantum number, which we have assigned to the Dirac cones. An enlarged figure of the QAH state is given in Fig. 3.

SVPM states, the conduction and valence bands touch the Fermi surface both at the K and K' points. We expect topological quantum critical phenomena in these states.

In order to explore the physics underlying the phase diagram, we analyze the low-energy effective Hamiltonian derived from the tight binding model (1). It is described by the Dirac theory around the K_η point as

$$H_\eta = \hbar v_{\rm F}(\eta k_x \tau_x + k_y \tau_y) + \eta \tau_z h_{11} - \ell E_z \tau_z + M\sigma_z + \lambda_{\rm R1}(\eta \tau_x \sigma_y - \tau_y \sigma_x)/2, \quad (2)$$

with $h_{11} = \lambda_{\rm SO}\sigma_z + a\lambda_{\rm R2}(k_y\sigma_x - k_x\sigma_y)$, where τ_a is the Pauli matrix of the sublattice pseudospin, $v_{\rm F} = \frac{\sqrt{3}}{2}at$ is the Fermi velocity, and $a = 3.86$ Å is the lattice constant.

The Hamiltonian H_+ explicitly reads

$$\begin{pmatrix} E(1,1) & \hbar v_{\rm F} k_- & ia\lambda_{\rm R2}k_- & 0 \\ \hbar v_{\rm F} k_+ & E(1,-1) & -i\lambda_{\rm R1} & -ia\lambda_{\rm R2}k_- \\ -ia\lambda_{\rm R2}k_+ & i\lambda_{\rm R1} & E(-1,1) & \hbar v_{\rm F} k_- \\ 0 & ia\lambda_{\rm R1}k_+ & \hbar v_{\rm F} k_+ & E(-1,-1) \end{pmatrix} \quad (3)$$

in the basis $\{\psi_{A\uparrow}, \psi_{B\uparrow}, \psi_{A\downarrow}, \psi_{B\downarrow}\}^t$, where $k_\pm = k_x \pm ik_y$, and the diagonal elements are

$$E(s_z, t_z) = \lambda_{\rm SO} s_z t_z - \ell E_z t_z + M s_z, \quad (4)$$

with the spin $s_z = \pm 1$ and the sublattice pseudospin $t_z = \pm 1$. They are not good quantum numbers in general. However, since $\lambda_{\rm R1}$ and $\lambda_{\rm R2}$ are very small with respect to the other parameters, it is a good approximation to set $\lambda_{\rm R1} = \lambda_{\rm R2} = 0$ in most cases. Thus, the spin s_z is almost a good quantum number in general. An exceptional case occurs when two Dirac cones collapse and cross each other, forming a QAH state after taking into account the effect of $\lambda_{\rm R2} \neq 0$, as we soon discuss.

We diagonalize the Hamiltonian (3) and obtain four energy levels. When two energy levels coincide, the band

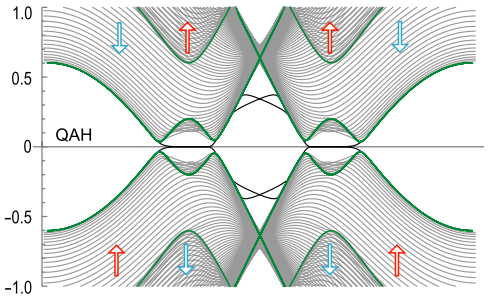

FIG. 3 (color online). The energy spectrum of a QAH state. Gray curves are for a nanoribbon, which are identical to Fig. 2 (QAH). Heavy green curves represent the energy spectrum of the bulk, calculated independently. A gap opens in the bulk spectrum, where almost flat gapless modes appear at the edges of a nanoribbon. A red (blue) arrow indicates the spin direction away from the Fermi level.

gap becomes zero, as found in Fig. 2 (M, VMP3, VMP2, SVPM). This occurs at the K and K' points, where $k_\pm = 0$. Let us temporarily neglect λ_{R1} because it is very small. Then, the band closes when $E(s_z, t_z) = E(s'_z, t'_z)$ with (4). They yield four lines described by $E_z = \pm\lambda_{SO}/\ell$ for $|M| \le \lambda_{SO}$, $M = \pm\lambda_{SO}$ for $|E_z| \le \lambda_{SO}/\ell$, and two lines by $M = \pm(\ell\lambda_{SO}/\lambda_{SO})E_z$ outside the square. They are illustrated by dotted lines in Fig. 1. These lines are modified by the nonzero effect of λ_{R1}, but the modification is too small to be recognized in Fig. 1. See also (5) for the typical order of correction.

The Hamiltonian can be diagonalized analytically in some cases. First, along the E_z axis in the phase diagram (Fig. 1), we have already demonstrated [7] that a topological phase transition occurs along the E_z axis from the QSH insulator [Fig. 2 (QSH)] to the band insulator [Fig. 2 (BI)]. The critical point is given by

$$E_c = \pm\frac{2\lambda_{SO}}{\ell}\left[\frac{\sqrt{1+(\alpha/\ell)^2}-1}{(\alpha/\ell)^2}\right], \tag{5}$$

where we have set $\lambda_{R1}(E_z) = \alpha E_z$ with $\alpha = 10^{-3}$ Å. Note that the effect of λ_{R1} is negligible, $(\alpha/\ell)^2 = 10^{-4}$. The SVPM realizes at the critical point, where helical currents flow in the bulk.

Second, along the M axis, the first Rashba interaction vanishes ($\lambda_{R1} = 0$), and the energy spectrum reads

$$\mathcal{E} = \pm\sqrt{a^2\lambda_{R2}^2k^2 + (M - s\sqrt{\lambda_{SO}^2 + \hbar^2v_F^2k^2})^2}. \tag{6}$$

We study a topological phase transition along the M axis based on this formula (6). When $M = 0$, there are two spin-degenerate Dirac cones for conduction and valence bands with a gap between them [Fig. 2 (QSH1)]. As M increases, the spin-up (spin-down) Dirac cones are pushed upward (downward) [Fig. 2 (QSH2)]. When $|M| \le \lambda_{SO}(1 + a^2\lambda_{R2}^2/\hbar^2v_F^2)$, the band gap is given as $\Delta = |M - s\lambda_{SO}|$ at $k = 0$, and it closes at $M = s\lambda_{SO}$: This is a topological phase transition point [Fig. 2 (M)]. Let us temporally assume $\lambda_{R2} = 0$. Then, as $|M|$ increases further, the two Dirac cones cross each other making a circle around each K_μ point. Actually, the Rashba interaction ($\lambda_{R2} \neq 0$) mixes up and down spins, turning the crossing points into the anticrossing points, and opens a gap to form the QAH insulating state [Fig. 2 (QAH) and Fig. 3].

When $|M| > \lambda_{SO}(1 + a^2\lambda_{R2}^2/\hbar^2v_F^2)$, the gap is given by

$$\Delta = a\lambda_{R2}\sqrt{\frac{M^2}{\hbar^2v_F^2 + a^2\lambda_{R2}^2} - \frac{\lambda_{SO}^2}{\hbar^2v_F^2}} \tag{7}$$

at

$$k_{ac} = \frac{\sqrt{\hbar^4v_F^4(M^2 - \lambda_{SO}^2) - a^2\lambda_{R2}^2\lambda_{SO}^2(2\hbar^2v_F^2 + a^2\lambda_{R2}^2)}}{\hbar v_F(\hbar^2v_F^2 + a^2\lambda_{R2}^2)}. \tag{8}$$

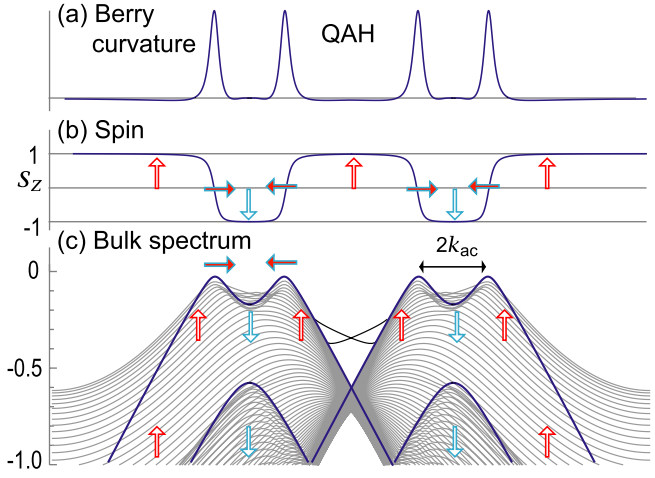

FIG. 4 (color online). (a) Berry curvature, (b) spin, and (c) band structure of a QAH state calculated based on formula (6) in the Dirac theory. Gray curves represent the energy spectrum of a nanoribbon, which are identical to Fig. 3. Spins rotate by the Rashba interaction near the Fermi level, generating a Skyrmion spin texture in the momentum space. It generates a nontrivial Berry curvature along the anticrossing circle whose radius given by (8). The integration of the Berry curvature gives the Chern number $C = 2$, since there are two Skyrmions each of which yields $C = 1$.

We present the energy spectrum (6) and the Berry curvature calculated by using the corresponding wave function at $M = 2\lambda_{SO}$ in Fig. 4. As explained there, spins rotates across the anticrossing point, generating a Skyrmion spin texture in the momentum space. This is consistent with the previous study for graphene [14]. The radius of the anticrossing circles is given by (8). We comment that the gap (7) is of the order of μeV when M is of the order of meV.

We now examine a point in the phase diagram such that $ME_z \neq 0$. In all regions where the effects of λ_{R1} and λ_{R2} are negligible, the energy spectrum is derived as

$$\mathcal{E} = s_zM \pm \sqrt{\hbar^2v_F^2k^2 + (\ell E_z - \eta s_z\lambda_{SO})^2}. \tag{9}$$

The effect of E_z is to change the mass of the Dirac electron. Let us increase E_z from $E_z = 0$ at a fixed value of M. The mass decreases (increases) for the Dirac cone characterized by $\eta s_z = +1$ ($\eta s_z = -1$) until $E_z = \lambda_{SO}/\ell$, but the behavior becomes opposite after $E_z = \lambda_{SO}/\ell$. As a result the tip of each Dirac cone is pushed either downward or upward as indicated in Fig. 2. Consequently the valley symmetry is broken. Note that the energy difference at each momentum $\hbar k$ between the conduction and valence bands with the same spin is given by

$$\Delta\mathcal{E}_\pm = 2\sqrt{\hbar^2v_F^2k^2 + (\ell E_z \mp \lambda_{SO})^2} \tag{10}$$

for $\eta s_z = \pm 1$, and this is independent of M. Thus, the difference is smaller for the up-spin Dirac cones at the K point, but this is opposite at the K' point.

We finally determine the phase boundary. It is determined as a boundary between insulating and metallic states. The Chern and spin-Chern numbers are quantized in insulating states, while they are ill defined in metallic states. As we have seen, each Dirac cone moves upward or downward oppositely at the K and K' points. Because of this phenomenon the system can become metallic though the gap is open both at the K and K' points. This is the VPM state. It occurs when one valence band crosses the Fermi level. The condition yields four heavy lines ($M = \pm\lambda_{\mathrm{so}} \pm \ell E_z$) in the phase diagram (Fig. 1). On the other hand, the gap formula (7) determines the boundary between the QAH phase and the VPM phase, which are the parabolic curves in the phase diagram (Fig. 1). In passing, we comment that the VPM phase is metallic in nature and does not have mobility gap. Thus, the transition from insulator to VPM might accompany a mobility gap closing.

I am very much grateful to N. Nagaosa for many fruitful discussions on the subject. This work was supported in part by Grants-in-Aid for Scientific Research from the Ministry of Education, Science, Sports and Culture No. 22740196.

[1] B. Lalmi, H. Oughaddou, H. Enriquez, A. Kara, S. Vizzini, B. Ealet, and B. Aufray, Appl. Phys. Lett. **97**, 223109 (2010).
[2] P. Vogt, P. De Padova, C. Quaresima, J. Avila, E. Frantzeskakis, M. C. Asensio, A. Resta, B. Ealet, and G. L. Lay, Phys. Rev. Lett. **108**, 155501 (2012).
[3] C.-L. Lin, R. Arafune, K. Kawahara, N. Tsukahara, E. Minamitani, Y. Kim, N. Takagi, and M. Kawai, Appl. Phys. Express **5**, 045802 (2012).
[4] K. Takeda and K. Shiraishi, Phys. Rev. B **50**, 14916 (1994).
[5] C.-C. Liu, W. Feng, and Y. Yao, Phys. Rev. Lett. **107**, 076802 (2011).
[6] C.-C. Liu, H. Jiang, and Y. Yao, Phys. Rev. B **84**, 195430 (2011).
[7] M. Ezawa, New J. Phys. **14**, 033003 (2012).
[8] M. Ezawa, J. Phys. Soc. Jpn. **81**, 064705 (2012).
[9] M. Z. Hasan and C. Kane, Rev. Mod. Phys. **82**, 3045 (2010).
[10] X.-L. Qi and S.-C. Zhang, Rev. Mod. Phys. **83**, 1057 (2011).
[11] C. L. Kane and E. J. Mele, Phys. Rev. Lett. **95**, 226801 (2005).
[12] C. Wu, B. A. Bernevig, and S.-C. Zhang, Phys. Rev. Lett. **96**, 106401 (2006).
[13] Z. Qiao, S. A. Yang, W. Feng, W.-K. Tse, J. Ding, Y. Yao, J. Wang, and Q. Niu, Phys. Rev. B **82**, 161414R (2010).
[14] W. K. Tse, Z. Qiao, Y. Yao, A. H. MacDonald, and Q. Niu, Phys. Rev. B **83**, 155447 (2011).
[15] Y. Yang, Z. Xu, L. Sheng, B. Wang, D. Y. Xing, and D. N. Sheng, Phys. Rev. Lett. **107**, 066602 (2011).
[16] M. Onoda and N. Nagaosa, Phys. Rev. Lett. **90**, 206601 (2003).
[17] C.-X. Liu, X.-L. Qi, X. Dai, Z. Fang, and S.-C. Zhang, Phys. Rev. Lett. **101**, 146802 (2008).
[18] Z. Qiao, H. Jiang, X. Li, Y. Yao, and Q. Niu, Phys. Rev. B **85**, 115439 (2012).
[19] J. Ding, Z. Qiao, W. Feng, Y. Yao, and Q. Niu, Phys. Rev. B **84**, 195444 (2011).
[20] H. Min, J. E. Hill, N. A. Sinitsyn, B. R. Sahu, L. Kleinman, and A. H. MacDonald, Phys. Rev. B **74**, 165310 (2006).
[21] D. N. Sheng, Z. Y. Weng, L. Sheng, and F. D. M. Haldane, Phys. Rev. Lett. **97**, 036808 (2006).
[22] E. Prodan, Phys. Rev. B **80**, 125327 (2009).